Article

Electron deficiency of nitro group determines hepatic cytotoxicity of nitrofurantoin

Hui Li, Zhengyu Zhang, Xiaojing Yang, Xu Mao, Ying Wang, Jian Wang, Ying Peng, and Jiang Zheng

Chem. Res. Toxicol., **Just Accepted Manuscript** • DOI: 10.1021/acs.chemrestox.8b00362 • Publication Date (Web): 19 Feb 2019

Electron deficiency of nitro group determines hepatic cytotoxicity of nitrofurantoin

Hui Li[†], Zhengyu Zhang[†], Xiaojing Yang[†], Xu Mao[†], Ying Wang[∥], Jian Wang[§], Ying Peng[†*], Jiang Zheng[†,‡*]

[†]Wuya College of Innovation, Shenyang Pharmaceutical University, Shenyang, Liaoning, 11016, P. R. China; [‡]State Key Laboratory of Functions and Applications of Medicinal Plants, Key Laboratory of Pharmaceutics of Guizhou Province, Guizhou Medical University, Guiyang, Guizhou, 550004, P. R. China; [§] School of Pharmaceutical Engineering, Shenyang Pharmaceutical University, Shenyang, Liaoning, 11016, P. R. China; [∥] School of Traditional Chinese Materia Medica, Shenyang Pharmaceutical University, Shenyang, Liaoning, 11016, P. R. China

[*]**Corresponding Author:**
Jiang Zheng, Shenyang Pharmaceutical University, No. 103, Wenhua Road, Shenyang, Liaoning, 110016, P. R. China. State Key Laboratory of Functions and Applications of Medicinal Plants, Key Laboratory of Pharmaceutics of Guizhou Province, Guizhou Medical University, Guiyang, Guizhou, 550004, P. R. China.
Email: zhengneu@yahoo.com
Tel: +86-24-23986361; Fax: +86-24-23986510.

Ying Peng, Shenyang Pharmaceutical University, No. 103, Wenhua Road, Shenyang, Liaoning, China.
Email: yingpeng1999@163.com
Tel: +86-24-23986361; Fax: +86-24-23986510.

†,‡: the two corresponding units contributed equally to this work.

Table of Contents graphic

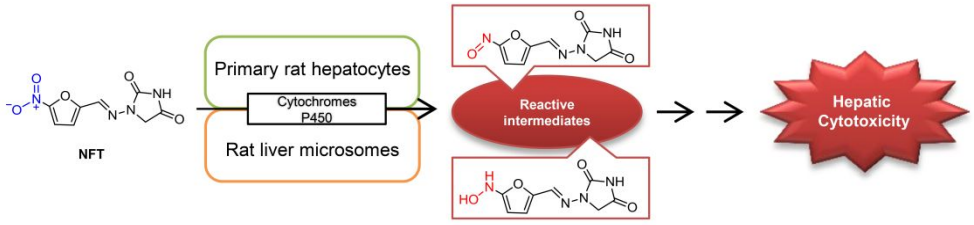

Abstract

Nitrofurantoin (NFT) is a widely used antimicrobial agent in the treatment of specific urinary tract infections (UTIs). Many adverse effects associated with NFT use have been reported, including hepatotoxicity. A structure-toxicity relationship study was performed to gain the insight into the mechanisms of toxic action of NFT. The toxic effects of NFT and its nine analogues or constituent moieties (**1**-**9**) designed and synthesized by structural manipulation of NFT were evaluated in rat liver microsomes and primary rat hepatocytes. A decrease in ability to deplete glutathione (GSH) was found in the following order: nitrofuran-containing compounds (NFT and **1**-**3**) > nitrobenzene-containing compounds (**4**-**5**) > nitro-free compounds (**6**-**9**). Similar pattern was observed in the cytotoxicity of these compounds as that of GSH depletion. The potential for reduction (electron deficiency) of nitro groups of the nitro-containing test compounds (NFT, **1**-**5**) decreased with the decrease in the ability to deplete GSH and the intensity of their cytotoxicity. The corresponding nitroso and hydroxylamine intermediates resulting from metabolic reduction of NFT were found to be reactive to GSH for the first time. Additionally, nitro-containing compound **4** (a model compound) was much more cytotoxic than the corresponding analine (**4a**). The findings allowed us not only to define the mechanism of toxic action of NFT but also to provide medicinal chemists with instructive guidance for rational design of nitro-containing pharmaceutical agents.

Introduction

Nitrofurans are commonly used as antibiotics and food additives in many countries. The potentially mutagenic and carcinogenic effects and the ambiguous mechanisms have drawn broad attention.[1] As a 5-nitrofuran derivative, nitrofurantoin (NFT), (1-{[(5-nitro-2-furanyl)methylene]amino}-2,4-imidazolidinedione), is an antimicrobial agent and has been widely used for almost seven decades in the first-line treatment of uncomplicated urinary tract infections (UTIs).[2,3] However, various adverse effects have been observed arising from the long-term use of NFT, including hepatotoxicity which was characterized by acute hepatitis, granulomatous reaction, cholestasis, autoimmune-mediated hepatitis and chronic active hepatitis.[4,5] And NFT-associated liver injury is also known as one of the most common causes of drug induced liver injury (DILI).[6] Numerous liver injury cases due to NFT use have been reported, even including a number of deaths.[7-12] Thus, clarifying the mechanisms is very urgent for assessment of its adverse effects for its safe use.

As a member of 5-nitrofuran family, NFT contains a nitrofuran group and a hydantoin side chain (Figure 1, NFT). According to the previous studies, the 5-nitrofuran group is considered as a basic requirement for mutagenicity and carcinogenicity.[13] Reduction of the nitro group is a major metabolic pathway of NFT. It is presumed that the corresponding nitroso and hydroxylamine intermediates are likely to form covalent binding with bio-macromolecules, which may trigger toxicities.[14,15] The reactive intermediates of NFT via metabolic

reduction, however, have not been identified. Besides, the furan ring can also be bioactivated via epoxidation and the resulting electrophilic epoxide metabolite can react with nucleophilic sites of bio-macromolecules.[16-19] It is worth noting that the toxicities and mutagenicities of various nitrofurans are different by several orders, which appears that the hydantoin side chain of NFT may be responsible for the toxicities as well, not merely due to the common nitrofuran group.[20] Nevertheless, which structural element within NFT plays a key role in liver injury is still largely unknown. The objectives of the present study were to define the critical element responsible for NFT-induced hepatotoxicity by dissecting the structure of NFT, to determine the importance of electrophilicity of nitro groups in cytotoxicity of nitroaromatic compounds, and to characterize reactive metabolites responsible for NFT-induced toxicities.

Materials and methods

2.1 Chemicals and materials

NFT (>98%), furfural, benzaldehyde, 5-nitro-2-furaldehyde, 3-nitrobenzaldehyde, *p*-nitrobenzaldehyde, hydrazine monohydrate, methylhydrazine sulfate and tin chloride dihydrate ($SnCl_2 \cdot 2H_2O$) were supplied by Aladdin Industrial Corporation (Shanghai, China). Hydantoin (99%) was gained from J&K Scientific Ltd. (Beijing, China). 1,1-Dimethylhydrazine hydrochloride was offered by Sam Chemical Technology Co., Ltd. (Shanghai, China). Glutathione (GSH), *S*-hexylglutathione, NADPH, oxidized glutathione (GSSG), monobromobimane (mBrB), collegenase Ⅱ and Dulbecco's Modified Eagle Medium (DMEM) were purchased from Sigma Aldrich (St. Louis, MO). 1-Aminohydantoin hydrochloride (>98%), percoll and rat tail tendon collagen type Ⅰ were obtained from Dalian Meilun Biotechnology Co., LTD. (Dalian, China). Thiazolyl blue tetrazolium bromide (MTT) was provided by Acros organics (Morris Plains, NJ). Rat liver microsomes (RLMs) (Sprague-Dawley, male) were prepared in our laboratory, according to a previously published method.[21] All organic solvents were purchased from Fisher Scientific (Springfield, NJ). All of the reagents and solvents were of analytical or HPLC grade.

2.2 Chemical synthesis

2.2.1 General chemistry

All commercial reagents and solvents were used directly without further purification. ^{1}H NMR spectra were obtained on a Bruker 600 MHz spectrometer.

Spectral data were recorded as follows: chemical shift (δ, as ppm referenced to TMS), multiplicity (s = singlet, d = doublet, dd = double doublets, t = triplet, m = multiplet), coupling constant (J, as Hz), and integration value. High resolution mass spectra (HRMS) were obtained with a hybrid quadrupole time-of-flight (Q-TOF) mass spectrometer (Bruker microQ-TOF, Germany) with an ESI source in positive mode. Purity of the test compounds was estimated by HPLC-analysis with an Eclipse Plus C18 column (5 μm, 150 mm×4.6 mm; Agilent, USA) and UV detection at 254 nm on a 1260 infinity system (Agilent Technologies, Santa Clara, CA). Analytical conditions were as follows: solvent A: acetonitrile with 0.1% (v/v) formic acid; solvent B: water with 0.1% (v/v) formic acid; flow rate: 0.8 ml/min; linear gradient program, 10% A 1-2 min, 10-90%A 2-10 min, 90%A 10-12 min, 90-10%A 12-14 min, 10%A 14-15 min; column temperature, 25 °C. The purity of all tested compounds was at least 95%. Reported yields were not optimized, since the focus is on purity of products rather than quantity.

2.2.2. General procedure for the synthesis of compound 1-7

Aldehydes (1.0 equiv) dissolved in methanol and the corresponding hydrazines (1.1-2.0 equiv) in water were mixed, and the resultant mixtures were stirred at room temperature in the dark, respectively. The resulting precipitates were filtered, washed twice with ice-cold methanol and water, and finally, dried at room temperature to give **1-7**.

5-Nitro-2-furancarboxaldehyde hydrazone (1)

The reaction was carried out as previously reported, with some modifications，as the general procedure described above.[22,23] Compound **1** (yield 66%) was obtained as a yellow solid. ^{1}H NMR (600 MHz, DMSO-d_6): δ8.01 (s, 2H), 7.71 (d, J=4.0 Hz, 1H), 7.57 (s, 1H), 6.75 (d, J= 4.0 Hz, 1H). HRMS: $[M + Na]^+$ *m/z* calcd 178.0223, found 178.0225, err -1.0 ppm.

5-Nitro-2-furancarboxaldehyde methylhydrazone (2)

The title compound (yield 42%) as an orange solid was prepared, according to the general procedure with an additional neutralization step of methylhydrazine sulfate with NaOH before the reaction. ^{1}H NMR (600 MHz, DMSO-d_6): δ8.65 (q, J=4.0 Hz, 1H), 7.72 (d, J=4.0 Hz, 1H), 7.24 (s, 1H), 6.71 (d, J= 4.0 Hz, 1H), 2.87 (d, J=3.8 Hz, 3H). HRMS: $[M + Na]^+$ *m/z* calcd 192.0380, found 192.0383, err -2.0 ppm.

5-Nitro-2-furancarboxaldehyde dimethylhydrazone (3)

The methods reported by Kevin T. Potts et al. and Etienne Pair et al. were followed with some modifications, as the general procedure described above.[24,25] Compound **3** (yield 75%) was obtained as a red solid. ^{1}H NMR (600 MHz, DMSO-d_6): δ7.72 (d, J=4.0 Hz, H), 7.11 (s, 1H), 6.69 (d, J=4.0 Hz, 1H), 3.09 (s, 6H). HRMS: $[M + Na]^+$ *m/z* calcd 206.0536, found 206.0544, err -4.1 ppm.

1-[[(4-Nitrophenyl)methylene]amino]-2,4-imidazolidinedione (4)

Compound **4** (yield 80%) as a white solid was prepared following the general procedure. ^{1}H NMR (600 MHz, DMSO-d_6): δ11.39 (s, 1H), 8.32 (d, J=8.9 Hz, 2H),

7.94 (d, J= 8.9 Hz, 2H), 7.92 (s, 1H), 4.38 (s, 2H). HRMS: $[M + Na]^+$ *m/z* calcd 271.0438, found 271.0444, err -2.2 ppm.

1-[[(3-Nitrophenyl)methylene]amino]-2,4-imidazolidinedione (5)

Compound **5** (yield 76%) as a white solid was prepared following the general procedure. ^1H NMR (600 MHz, DMSO-d_6): δ11.36 (s, 1H), 8.50 (s, 1H), 8.25 (dd, J=8.1, 2.20Hz, 1H), 8.12 (d, J=7.8 Hz, 1H), 7.97 (s, 1H), 7.76 (t, J=8.0, 8.0 Hz 1H), 4.37 (s, 2H). HRMS: $[M + Na]^+$ *m/z* calcd 271.0438, found 271.0433, err 1.7 ppm.

1-[(2-Furanylmethylene)amino]-2,4-imidazolidinedione (6)

Compound **6** (yield 51%) as a white solid was prepared following the general procedure. ^1H NMR (600 MHz, DMSO-d_6): δ11.24 (s, 1H), 7.82 (d, J=1.2 Hz, 1H), 7.69 (s, 1H), 6.83 (d, J= 3.4 Hz, 1H), 6.62 (dd, J=3.4, 1.8 Hz, 1H), 4.31 (s, 2H). HRMS: $[M + Na]^+$ *m/z* calcd 216.0380, found 216.0388, err -3.9 ppm.

1-[(2-Phenylmethylene)amino]-2,4-imidazolidinedione (7)

Compound **7** (yield 73%) as a white solid was prepared following the general procedure. ^1H NMR (600 MHz, DMSO-d_6): δ11.25 (s, 1H), 7.80 (s, 1H), 7.70 (m, 2H), 7.43 (m, 3H), 4.36 (s, 2H). HRMS: $[M + Na]^+$ *m/z* calcd 226.0587, found 226.0597, err -4.5 ppm.

2.2.3 Synthesis of

1-[[(4-Aminophenyl)methylene]amino]-2,4-imidazolidinedione(4a)

Compound **4a** was obtained by reduction of **4** (30 mg, 0.12 mmol) with $SnCl_2 \cdot 2H_2O$ (110 mg, 0.49 mmol) in concentrated HCl (2 mL) as previously

reported.[26] Compound **4a** (3 mg, 11%) was obtained as a yellow solid. ^{1}H NMR (600 MHz, DMSO-d_6): δ11.09 (s, 1H), 7.60 (s, 1H), 7.36 (d, J= 8.5 Hz, 2H), 6.57 (d, J= 8.5 Hz, 2H), 5.59 (s, 2H), 4.30 (s, 2H). HRMS: $[M + Na]^+$ *m/z* calcd 241.0696, found 241.0705, err -3.8 ppm.

2.3 Microsomal incubations of NFT

The incubation mixtures containing 100 μM NFT, 1.0 mg/mL rat liver microsomal protein, 10.0 mM GSH and 3.2 mM $MgCl_2$ were prepared in potassium phosphate buffer (PBS, pH 7.4) in the presence or absence (control) of NADPH. The reactions were initiated by addition of NADPH (final concentration: 1.0 mM) to the mixture. After incubation for 30 min at 37 °C, the reactions were quenched by mixing with an equal volume of ice-cold acetonitrile, followed by vortexing for 1 min and centrifuging at 19 000 g for 10 min at 4 °C to remove the precipitated proteins. A 5 μL aliquot of the resulting supernatants was loaded into liquid chromatography coupled with tandem mass spectrometry (LC-MS/MS) system for analysis. Stock solution of NFT was prepared in DMSO.

2.4 GSH and GSSG assessment in microsomal incubations

The GSH and GSSG assays in microsomal incubations were performed as previously reported.[27,28] The incubation mixtures (final volume: 250 μL) contained 1.0 mM individual test compounds (NFT, **1-7** or **4a**), 2.0 mg/mL rat liver microsomal protein, 200 μM GSH and 3.2 mM $MgCl_2$. NADPH (1.0 mM) was added to start the reaction, followed by incubating for 30 min at 37 °C. The amount of GSH

remaining in the protein-free supernatants was measured by the method established by our lab, with some modifications.[29] Briefly, aliquots of the resulting incubation mixtures (30 μL) were moved to another Eppendorf vials containing 50 μL ice-cold acetonitrilic mBrB (2.2 mM) to stop the reactions together with chemical derivatization. Particularly, the derivatization reactions were conducted in the dark at room temperature for 1 h to produce the mBrB-derived GSH conjugate.[30] The resulting derivatization samples were spiked with 110 μL PBS and 10 μL of *S*-hexylglutathione (in acetonitrile, internal standard, final concentration: 0.3 μM). After centrifuging at 19,000g for 10 min, the supernatants (5 μL) were subjected to LC-MS/MS for analysis.[29] The results were corrected for loss of GSH (formation of GSSG) resulting from auto-oxidation. Comparisons were made relative to the control and contents of GSH, GSSG or loss of GSH, and expressed as the percentage of the control, respectively.

2.5. Isolation and culture of primary rat hepatocytes

The study was approved by the Institutional Animal Ethical Committee of Shenyang Pharmaceutical University. Male Sprague-Dawley rats (280-300 g) were fed with a standard chow diet and water *ad libitum*. Primary rat hepatocytes were prepared, according to a two-step collagenase perfusion method.[31] The viability was always higher than 90% as determined by trypan blue exclusion. Isolated hepatocytes were seeded at a density of 1.5×10^5 cells/mL on collagen-precoated 96-well plates, followed by culture for 4 h at 37 °C under a humidified atmosphere (95% O_2 and 5% CO_2) in DMEM which contains 20% fatal bovine serum (FBS), 200

U/ml penicillin-streptomycin, 0.09 μM insulin and 0.1 μM dexamethasone.

2.6 Cytotoxicity measured by the MTT assay

Cells were incubated for 4 h in serum-free DMEM containing NFT, **1-9** or **4a** (500 μM). Microplates were then rinsed with EDTA-free PBS (pH 7.4) and the cell viability was determined using the MTT assay, according to the method described by Mosmann.[32] Stock solutions of individual test compounds (0.5 M) were prepared in DMSO (final concentration in the media, 0.1%), and vehicle control was performed using DMSO (0.1%) only.

2.7 Computational details

All theoretical calculations were carried out using the SYBYL Versions 6.91 (SYBYL® 6.9.1 Tripos Inc., St. Louis, USA) molecular modeling software. All molecular electrostatic potential (MEP) calculations and visualization were performed using the MOLCAD program. Partial atomic charges of the nitro-containing test compounds were calculated by the Gasteiger-Hückel method.

2.8 LC-MS/MS method

NFT-derived GSH conjugates were analyzed on an AB SCIEX Instruments 5500 triple quadrupole mass spectrometer (Applied Biosystems, Foster City, CA) interfaced online with a 1260 infinity system (Agilent Technologies, Santa Clara, CA). Chromatographic separation was performed from an Eclipse Plus C18 column (5 μm, 150 mm×4.6 mm; Agilent, USA) by gradient elution with a flow rate of 0.8 mL/min. The mobile phases were composed of 0.1% (v/v) formic acid in

acetonitrile (A) and 0.1% (v/v) formic acid in water (B). The linear gradient was as follows: 10% A at the first 2 min; linear gradient from 10% to 90% A in 8 min; 90% A step for 2 min; back to 10% A in 2 min; 10% A step for 1 min. The total analysis time was 15 min. Conjugates were analyzed in positive ion mode by MRM mode. The mass spectrometric instrument parameters were set as follows: ion source temperature (TEM) was at 650°C; ion spray voltage (IS) and entrance potential (EP) were 5500 and 10 V, respectively; curtain gas (CUR), gas 1 (GS1) and gas 2 (GS2) were 35, 50 and 50 psi, respectively. The characteristics of ion pairs (corresponding to declustering potential DP, collision energy CE, collision cell exit potential CXP) were *m/z* 530/308 (90, 30, 13) and 514/162 (100, 35, 14) for the GSH conjugates.

Additionally, AB SCIEX Instruments 4000 Q-Trap™ (Applied Biosystems, Foster City, CA) interfaced online with a 1260 infinity system (Agilent Technologies, Santa Clara, CA) were used and the NFT-derived GSH conjugates were analyzed by multiple-reaction monitoring-information-dependent acquisition-enhanced product ion (MRM-IDA-EPI) scan mode. IDA was used to trigger acquisition of EPI spectra for ions exceeding 500 cps with exclusion of former target ions after three occurrences for 10 s. The EPI scan was also run in positive mode at a scan range for product ions from *m/z* 50 to 550. The CE was set at 40 eV with a spread of 15 eV. Other instrument parameters were equivalent to those described above. The operation conditions for determining the contents of GSH and GSSG were in accordance with the method described previously with an addition of the ion pair *m/z* of 613.1/355.0 (115, 30, 3) for GSSG.[29] All data were analyzed using the AB

SCIEX Analyst 1.6.3 software (Applied Biosystems).

A fourier transform-ion cyclotron resonance (FT-ICR) mass spectrometer (Bruker Solarix 7.0T, Germany) with an ESI source equipped with an Agilent 1260 LC system was also employed to characterize the NFT-derived GSH conjugates. The optimized parameters of electrospray ionization-mass spectrometry (ESI-MS) were as follows: nebulizer gas pressure (4.0 bar), dry gas flow rate (8.0 L/min) and temperature (200°C), ion accumulation time (0.15 s), time of flight (0.6 ms), capillary voltage (4.5 kV), and end plate offset (500 V). The full scan MS data were acquired over a range of *m/z* 100-1000 in positive mode. LC conditions were similar to those described above. Data Analysis Software (Bruker, Germany) was used for data analysis.

2.9 Statistical Analysis.

Data are expressed as the mean±S.D. of triplicate samples. Statistical significance of differences between treatment groups in these studies was evaluated with the Student's t test and differences were considered significant at $p<0.05$.

Results

3.1 GSH depletion by NFT and 1-9 in rat liver microsomal incubations.

The levels of GSH and GSSG in microsomes after 30 min incubation of individual test compounds (NFT, **1-9**) in the presence of NADPH are shown in Figure 2. As for the full range of incubation systems, the decrease of GSH accompanied with the formation of GSSG and the lower the contents of GSH remained, the more the GSSG detected, suggesting that the observed GSH depletion resulted from the formation of GSSG. Besides, the levels of GSH showed an increasing tendency in NFT, **1-9** treated samples, ranging from 14.0% to 98.5% when compared with control. In other words, a decrease in ability to deplete GSH was found in the following order: nitrofuran-containing compounds (NFT and **1-3**) > nitrobenzene-containing compounds (**4-5**) > nitro-free compounds (**6-9**) (Figure 1 and Figure 3A). Nitro-containing compounds NFT and **1-5** were as much as 1.75-58 fold more potent to deplete GSH than nitro-free compounds **6-9**. The potencies of NFT and **4** or **5** for GSH depletion were about 4 and 30 or 23 times higher than that of the corresponding nitro-free **6** and **7,** respectively. Furthermore, 83%, 45% and 35% GSH were depleted when treated with NFT, **4** and **5**, respectively, indicating that the replacement of furan ring with a phenyl ring resulted in approximately 50% loss of the ability to deplete GSH.

3.2 Cytotoxicity of NFT and 1-9 in primary rat hepatocytes

Cytotoxicities of NFT and **1-9** were evaluated in primary rat hepatocytes. Cells were exposed to the individual test compounds at 500 μM, a cytotoxic concentration

of NFT.[33] Nitrofuran derivatives NFT and **1-3** were found to be more toxic than nitrobenzene derivatives **4-5** (Figure 1 and 4A), which coincides with that of the GSH depletion assay (Figure 1, 3A and 4A).

3.3 Computer simulation

To gain a better understanding of the relationship between the chemical reactivity of nitro-containing compounds (NFT, **1-5**) and their toxicities, MEP and partial atomic charges on nitrogen of the nitro groups of the test compounds were calculated. MEP contour maps show that the region near the nitrogen atom of nitro group of NFT is more positive than those of the corresponding **4** and **5**, a range of 22.7-29.9 kcal/mol versus 1.2-8.4 kcal/mol (Figure 5), indicating higher nucleophilic susceptibility of NFT. As for the other three nitrofuran-containing compounds, **1-3**, the positive regions are merely over nitrogen atom of the nitro moieties of them, respectively, ranging from 29.9 to 51.4 kcal/mol, which show high electrophilic reactivity. Besides, the regions over furan rings of nitrofuran-containing compounds NFT and **1-3** are more positive than those of the phenyl rings of nitrobenzene-containing compounds **4** and **5**. Partial atomic charges on nitrogen of the nitro groups of NFT and **1-5** are shown in Figure 6. As expected, partial positive charges on nitrogen of the nitro groups of the listed compounds decreased in the following order: nitrofuran-containing compounds (**1-3** and NFT) > nitrobenzene-containing compounds (**4** and **5**), coinciding with MEP calculation.

3.4 Toxic role of nitro group of NFT

3.4.1 Formation of NFT-derived GSH conjugates in microsomal incubations.

Identification of reactive metabolites is a key step to define the mechanisms of toxic action of NFT. Reactive intermediates of NFT were trapped by GSH in microsomal incubations. The formation of the resulting GSH conjugates was monitored by LC-MS/MS. Two metabolites (M1 and M2) were detected and the formation of the two both appeared to be NADPH- and cytochrome P450 (P450)-dependent (Figure 7A, B, D and E).

M1, with the retention time at 2.27 min, was detected by scanning of the ion pair of *m/z* 530→308. The tandem mass (MS/MS) spectrum of M1 obtained through MRM-IDA-EPI scanning in positive mode is shown in Figure 7C. Major fragment ions at *m/z* 308.0, 223.0, 179.0, and 162.1 all resulted from the cleavage of GSH moiety, indicating the participation of GSH in the formation of M1. In detail, product ions at *m/z* 308.0 and 223.0 were generated from the protonation of GSH and a total loss of GSH (-307 Da) from *m/z* 530, respectively, arising from the cleavage of the N-S bond of M1. Another major ion at *m/z* 179.0 was derived from a loss of the *γ*-glutamyl moiety (-129 Da) from GSH and a sequential loss of NH_3 generated fragment ion at *m/z* 162.1.

M2, eluted at a retention time of 2.30 min, was detected by acquiring ion pair at *m/z* 514→162 in positive mode. The MS/MS spectrum of M2 exhibited the major fragment ions associated with fragmentation of the GSH moiety, signaling the participation of GSH (Figure 7F). Product ions at *m/z* 439.1 and 385.1 were obtained from the loss of the glycinyl moiety (-75 Da) and *γ*-glutamyl moiety (-129

Da) from *m/z* 514, respectively, and 367.1 was gained from an elimination of H_2O from *m/z* 385.1. The observed fragment ion at *m/z* 162.2 was generated as that of M1 described above.

Additionally, the incubation mixtures were also analyzed by high resolution mass spectrometry to characterize the elemental compositions of M1 and M2. The protonated molecular ions of these two conjugates were found to be 530.13174 and 514.13619, matching the formulas of $C_{18}H_{24}N_7O_{10}S$ and $C_{18}H_{24}N_7O_9S$, respectively (Figure 8 and Table 1). And the accurately measured mass in the high resolution mass spectrometry system was in accordance with the corresponding theoretical mass within 5 ppm based on the predicted formula and the similarity scores of the detected and predicted isotope patterns of M1 and M2 were both found to be 100, making the data more reliable (Table 1).

3.4.2 GSH depletion by 4 and 4a in microsomal incubations

To define the mechanisms of NFT-induced toxicities, the ability to deplete GSH of **4a**, an aniline analogue of **4**, was evaluated. Figure 3B shows that 45% GSH was depleted by **4**, whereas **4a** showed little GSH depletion property (only 0.6%). In other words, reduction of **4** to the corresponding aniline resulted in 99% decreased capability of GSH depletion.

3.4.3 Cytotoxicity of 4 and 4a in primary rat hepatocytes

Cytotoxicity study of **4** and **4a** was conducted in primary hepatocytes by the MTT assay. As expected, less cytotoxicity was found when cells were treated with

4a rather than **4**, as exhibited in Figure 4B, consistent with that of the GSH depletion assay.

Discussion

NFT, a nitrofuran derivative, has been applied for the first-line treatment of specific UTIs since 1950s.[2,3] However, since its introduction into clinical use, NFT has been associated with various adverse effects, including hepatotoxicity.[4,5] Though many efforts have been made to explore the insight into NFT-induced liver injury, little is known about the mechanisms, and even the group which plays a key role in this adverse drug reaction. In the present study, we conducted a structure-toxicity relationship study by structural dissection to determine the essential functional group(s) responsible for NFT-induced hepatotoxicity. A total of nine compounds were rationally designed and synthesized to probe the mechanism of toxic action of NFT. Basically, the structure-toxicity relationship study was designed to answer three questions, including 1) whether the hydantoin moiety plays a role in NFT toxicity; 2) whether the nitro group is essential for NFT toxicity; and 3) whether the furan ring is required for NFT toxicity.

GSH plays a crucial role in cytoprotection, acting as a nucleophile capture for reactive metabolites generated from xenobiotics. GSH depletion is known as an early biomarker of cytotoxicities. As an initial step of toxicity evaluation, we determined the ability of NFT and **1**-**9** to deplete GSH in microsomal incubation systems. The GSH depletion-based microsomal incubation system is often used to investigate metabolism-mediated mechanisms of toxic action.[27,28] The GSH reactivity associated with these test compounds ranked in the following order: **1**-**3** and NFT > **4**-**5** > **6**-**9**. It is interesting to find that these compounds can be divided into

three groups: nitrofuran-containing compounds (**1**-**3**, NFT), nitrobenzene-containing compounds (**4**-**5**), and nitro-free compounds (**6**-**9**), based on their ability to deplete GSH. In other words, the results showed that the nitrofuran-containing compounds demonstrated the greatest GSH depletion property, indicating that 5-nitrofuran moiety of NFT most likely elicited toxicities rather than the hydantoin side chain. The nitro-containing compounds (NFT, **4**/**5**) produced much higher responses than those of the corresponding nitro-free compounds (**6**, **7**) (approximately 4, 30/23 times higher), respectively, suggesting that nitro group played the essential role in NFT toxicity. Besides, when the furan moiety of NFT was replaced by a phenyl ring, that is, the nitrobenzene-containing compounds, the small structural alternation resulted in dramatic decrease in ability to deplete GSH. This indicates that the furan ring may be another factor regarding the toxicities.

As the second step, toxicity of the test compounds was evaluated in primary rat hepatocytes. The cytotoxicity of these compounds revealed similar pattern as observed in the GSH depletion study, which solidified the evidence obtained from the GSH depletion study. However, compound **6**, a nitro-free furan-containing compound, was found to be more cytotoxic than nitro-containing compound **5**. Our early studies demonstrated nitro-free furan-containing compounds underwent oxidation to form *cis*-enedials. The formation of oxidative metabolites is most likely responsible for their toxicities.[21,34,35] These furan compounds did not show much GSH depletion effects.[21,35] Therefore, we were not surprised by the exceptional finding. Additionally, no significant difference was observed in the degrees of GSH

depletion induced by NFT and compounds **1**-**3** (Figure 3A), whereas the cellular viability of NFT and compound **3** were both significantly higher than that of **1**-**2** (Figure 4A). Interestingly, compounds **1** and **2** appeared to be more toxic than NFT and compound **3**. This may suggest that the numbers of methyl substituents at the terminal nitrogen atom may play some role in the observed cytotoxicity besides the nitro group, and the addition of hydantion in the side chain made NFT less cytotoxic.

We speculated that the electron deficiency on the nitrogen of the nitro groups which can be dictated by the properties of neighboring functional groups (furan/phenyl ring) would determine the potential of GSH depletion and the potency of cytotoxicity. An attempt was made to estimate the electron deficiency by MEP and partial atomic charges calculation. The calculated MEP contour maps and the partial charges on nitrogen of the nitro groups of the test compounds showed that the nitrogen of the nitro groups of the nitrofuran-containing compounds possessed more positive potential than that of the nitrobenzene-containing compounds, indicating higher electrophilic reactivity of the nitrofuran-containing compounds than that of the nitrobenzene-containing compounds. This explains the observed greater cytotoxicity of the nitrofuran-containing compounds than that of the nitrobenzene-containing compounds.

The rates of reductive reactions are known to depend on the electron density of the reactants, and electron deficiency favors reductive reactions. Additionally, similar trends were found for the formation of GSSG, the contents of which were monitored at the same time in the GSH depletion study, revealing that the observed

GSH depletion resulted in the formation of GSSG.

We proposed that these nitro-containing compounds mainly undergo nitro-reductive metabolic pathways to deplete GSH, as shown in Scheme 1. It is likely that the nitro group is firstly reduced to a nitroso mediated by P450, and the GSH applied attacks at the nitrogen atom of the nitroso to form the resulting GSH conjugate, followed by nucleophilic attack through a second molecule of GSH to the hydroxylamine with a release of GSSG. The hydroxylamine may also react with a third molecule of GSH to form another GSH conjugate, and then undergoes sequential attack by the fourth molecule of GSH to the amine, releasing a second GSSG molecule. The more GSH is depleted, the more GSSG formed.

We characterized reactive metabolites of NFT trapped with GSH in microsomal incubations and monitored the formation of the corresponding GSH conjugates. Two products (M1 and M2) were detected by LC-MS/MS, which appeared to be NADPH and P450 dependent, suggesting that P450 enzymes played an important role in the metabolic reduction of the nitro group of NFT. There were two possible chemical structures of M1 we proposed at first, since the hydroxyl group of the semi-mercaptal may migrate to the sulfur atom to form a sulphinamide. However, the observed product ions of M1 at *m/z* 308.0 and 223.0, which were generated from the cleavage of the N-S bond, indicate that the hydroxyl group attaches to the nitrogen atom, and the formation of sulphinamide isomer of M1 is unlikely. Additionally, MS spectrum and elemental analysis demonstrated M2 contained one oxygen atom less than M1, suggesting M2 is a sulfenamide. This surprised us, since

semi-mercaptals may rearrange to the sulphinamides which are apparently more stable. Besides, aryl sulfenamides are notoriously unstable, while the semi-mercaptal form (M1) and sulfenamide form (M2) of NFT appeared to be unexpectedly stable. The characteristic fragment ions (mainly derived from the cleavage of GSH) and elemental compositions (characterized by high resolution mass spectrometry) confirmed the proposed structures of M1 and M2. NFT-induced decrease in cellular GSH contents has been documented, along with proposed metabolic reduction.[36-39] However, the mechanisms of the observed GSH depletion remain unknown. We succeeded in identifying the nitroso and hydroxylamine (Scheme 1) as the reactive intermediates responsible for the GSH depletion. The findings encouraged us to hypothesize that metabolic reduction of the nitro group to nitroso and hydroxylamine initiated GSH depletion and the development of toxicities. Besides, GSH depletion can also be attributed to redox recycling of the NFT nitro radical anion, which may trigger oxidative stress and lead to cytotoxicity as a consequence (Scheme 1). [36-39]

We made a great effort to chemically reduce NFT to the corresponding nitroso and amine, since we wanted to manipulate the electron density of the nitro group of NFT and to compare the relative toxicity of these compounds to provide additional evidence for our hypothesis. Unfortunately, we failed due to the unstability of the anticipating products. Then we successfully reduced **4** to its aniline analogue (**4a**) and employed **4** and **4a** for our mechanistic studies. As expected, **4a** was less toxic than **4**, which was found in both GSH depletion and cytotoxicity studies, suggesting

that the reductive process of nitro to the amine induces cytotoxicity and the nitro group plays a key role in cytotoxicity. It is likely that NFT underwent similar reductive metabolic pathway with the nitroaromatic moiety as that of **4** to trigger cytotoxicity. This also supports our hypothesis, since the more electron deficient nitro group is, the easier be reduced to the nitroso and hydroxylamine, and the faster to deplete GSH, followed by an increase in GSSG formation and cytotoxicity.

Conclusions

In conclusion, the key moiety in contribution to NFT cytotoxicity was the nitro group. The development of NFT cytotoxicity required metabolic reduction of its nitro group. The resulting nitroso and hydroxylamine intermediates were responsible for the observed GSH depletion and cytotoxicity induced by NFT. The electron deficiency of the nitrogen of the nitro group favored the cytotoxicity of nitroaromatic compounds. The findings of this study facilitate the understanding of the mechanisms of toxic action of nitroaromatic compounds and the development of nitroaromatic new drugs.

Funding Information

This work was supported in part by the National Natural Science Foundation of China [Grants 81773813, 81430086, 81830104].

Compliance with ethical standards

Conflict of interest

The authors declare that they have no conflict of interest.

Abbreviations list

CE, collision energy; CUR, curtain gas; CXP, collision cell exit potential; DILI, drug induced liver injury; DMEM, Dulbecco's Modified Eagle Medium; DP, declustering potential; EP, entrance potential; ESI-MS, electrospray ionization-mass spectrometry; FBS, fatal bovine serum; FT-ICR, fourier transform-ion cyclotron resonance; GSH, glutathione; GS1, gas 1; GS2, gas 2; GSSG, oxidized glutathione; IS, ion spray voltage; LC-MS/MS, liquid chromatography coupled with tandem mass spectrometry; mBrB, monobromobimane; MEP, molecular electrostatic potential; MRM-IDA-EPI, multiple-reaction monitoring information-dependent acquisition-enhanced product ion; MS/MS, tandem mass; MTT, thiazolyl blue tetrazolium bromide; NFT, nitrofurantoin; P450, cytochrome P450; PBS, potassium phosphate buffer; Q-TOF, hybrid quadrupole time-of-flight; RLMs, rat microsomes; $SnCl_2 \cdot 2H_2O$, tin chloride dehydrate; TEM, ion source temperature; UTIs, urinary tract infections.

References

[1] Van Koten-Vermeulen, J. E. M., Wouters, M. F. A., and Van Leeuwen, F. X. R. (1993) Toxicological evaluation of certain veterinary drug residues in food. Report of the 40th Meeting of the Joint FAO/WHO Expert Committee on Food Additives (JECFA). Geneva: World Health Organisation. pp. 85-123.

[2] Concia, E., Bragantini, D., and Mazzaferri, F. (2017) Clinical evaluation of guidelines and therapeutic approaches in multi drug-resistant urinary tract infections. *J. Chemother. 29*, 19-28.

[3] Moreno, S. N., Mason, R. P., and Docampo, R. (1984) Reduction of nifurtimox and nitrofurantoin to free radical metabolites by rat liver mitochondria. Evidence of an outer membrane-located nitroreductase. *J. Biol. Chem. 259*, 6298-6305.

[4] Sargın, G., Elbek, O., Balantekin, C., Meteoglu, İ., Culhacı, N. (2012) Acute respiratory distress syndrome and hepatotoxicity associated with single dose nitrofurantoin use: a case report. *Case. Rep. Pulmonol. 2012*, 465389.

[5] Sakaan, S. A., Twilla, J. D., Usery, J. B., Winton, J. C., Self, T. H. (2014) Nitrofurantoin-induced hepatotoxicity: a rare yet serious complication. *South Med. J. 107*, 107-113.

[6] https://livertox.nlm.nih.gov/Nitrofurantoin.htm (Access Date: 26th January 2019)

[7] Ernaelsteen, D., and Williams, R. (1961) Jaundice due to nitrofurantoin. *Gastroenterology 41*, 590-593.

[8] Ramadas, P., Krishnan, P., and Frechette, V. (2018) An Unusual Case of Nitrofurantoin-Associated Hepatotoxicity. *Am. J. Ther. 25*, e378-e379.

[9] Black, M., Rabin, L., and Schatz, N. (1980) Nitrofurantoin-induced chronic active hepatitis. *Ann. Intern. Med. 92*, 62-64.

[10] Hatoff, D. E., Cohen, M., Schweigert, B. F., Talbert, W. M. (1979) Nitrofurantoin: another cause of drug-induced chronic active hepatitis? A report of a patient with HLA-B8 antigen. *Am. J. Med. 67*, 117-121.

[11] Kiang, T. K., Ford, J. A., Yoshida, E. M., Partovi, N. (2011) Nitrofurantoin associated lung and liver toxicity leading to liver transplantation in a middle-aged patient. *Can. J. Hosp. Pharm. 64*, 262-270.

[12] Tolman, K. G. (1980) Nitrofurantoin and chronic active hepatitis. *Ann. Intern. Med. 92*, 119-120.

[13] McCalla, D. R. (1983) Mutagenicity of nitrofuran derivatives: review. *Environ. Mutagen. 5*, 745-765.

[14] Aufrère, M. B., Hoener, B. A., and Vore, M. (1978) Reductive metabolism of nitrofurantoin in the rat. *Drug Metab. Dispos. 6*, 403-411.

[15] Swaminathan, S., and Lower, G. J. (1978) Biotransformations and excretion of nitrofurans. In: *Carcinogenesis-A Comprehensive Survey, Volume 4, Nitrofurans*. (Bryan, G.T. Ed.) pp 59-97, Raven Press, New York.

[16] Li, H., Lin, D., Peng, Y., Zheng, J. (2017) Oxidative bioactivation of nitrofurantoin in rat liver microsomes. *Xenobiotica 47*, 103-111.

[17] Stepan, A. F., Walker, D. P., Bauman. J., Price, D. A., Baillie, T. A., Kalgutkar, A. S., Aleo, M. D. (2011) Structural alert/reactive metabolite concept as applied in medicinal chemistry to mitigate the risk of idiosyncratic drug toxicity: a

perspective based on the critical examination of trends in the top 200 drugs marketed in the United States. *Chem. Res. Toxicol. 24*, 1345-1410.

[18] Masubuchi, N., Makino, C., and Murayama, N. (2007) Prediction of in vivo potential for metabolic activation of drugs into chemically reactive intermediate: correlation of in vitro and in vivo generation of reactive intermediates and in vitro glutathione conjugate formation in rats and humans. *Chem. Res. Toxicol. 20*, 455-464.

[19] Mitchell, J. R., Snodgrass, W. R., and Gillette, J. R. (1976) The role of biotransformation in chemical-induced liver injury. *Environ. Health. Perspect. 15*, 27-38.

[20] Lu, C., McCalla, D. R., and Bryant, D. W. (1979) Action of nitrofurans on E coli: Mutation and induction and repair of daughter-strand gaps in DNA. *Mutat. Res. 67*, 133-144.

[21] Lin, D., Li, C., Peng, Y., Gao, H., Zheng, J. (2014) Cytochrome P450-mediated metabolic activation of diosbulbin B. *Drug Metab. Dispos. 42*, 1727-1736.

[22] Guerra, W., Fontes, A. P. S., Almeida, M. V. D., Silva, H. (2005) Synthesis and characterization of new platinum (II) complexes containing furan and nitrofuran derived ligands. *Quim. Nova. 28*, 809-812.

[23] Dudarev, V. G., Tikhomirova, O. M., and Iozep, A. A. (2013) Synthesis and antimicrobial activity of carboxymethylchitin derivatives. *Pharm. Chem. J. 47*, 31-34.

[24] Potts, K. T., and Walsh, E. B. (**1988**) Furan-2-carbaldehyde Dimethylhydrazones

in Diels-Alder Cycloadditions. *J. Org. Chem. 53*, 1199-1202.

[25] Pair, E., Monteiro, N., Bouyssi, D., Baudoin, O. (2013) Copper-Catalyzed Trifluoromethylation of N,N-Dialkylhydrazones. *Angew. Chem. Int. Ed. Engl. 52*, 5346-5349

[26] Sunagar, V. A., Latthe, P. R., and Badami, B. V. (2007) Azopyrazolobenzylidene Derivatives of 4-Amino-1,2,4-triazol-3-ones. Synthesis of 4-{[4-(3,5-Dimethyl-1*H*-pyrazol-4-yl)diazenyl]-benzylidene}amino-2-aryl-5-methyl-3*H*-[1,2,4]-triazol-3-ones. *J. Heterocyclic. Chem. 44*, 1-6.

[27] Garle, M. J., and Fry, J. R. (1989) Detection of reactive metabolites in vitro. *Toxicology 54*, 101-110.

[28] Rebecca, C. E., Garle, J. M., and Fry, R. J. (2000) Glutathione depletion in a liver microsomal assay as an in vitro biomarker for reactive metabolite formation. *Biomarkers 5*, 285-294.

[29] Yu, J., Li, C., Shen, S., Liu, X., Peng, Y., Zheng, J. (2015) Mass spectrometry based detection of glutathione with sensitivity for single-cell analysis. *Rapid Commun. Mass Spectrom. 29*, 681-689.

[30] Yang, C. S., Chou, S. T., Lin, N. N., Liu, L., Tsai, P. J., Kuo, J. S., Lai, J. S. (1994) Determination of extracellular glutathione in rat brain by microdialysis and high-performance liquid chromatography with fluorescence detection. *J. Chromatogr. B Biomed. Appl. 661*, 231-235.

[31] Seglen, P. O. (1976) Preparation of isolated rat liver cells. *Methods Cell Biol. 13*, 29-83.

[32] Mosmann, T. (1983) Rapid colorimetric assay for cellular growth and survival: application to proliferation and cytotoxicity assay. *J. Immunol. Methods 65*, 55-63.

[33] Silva, J. M., McGirr, L., and O'Brien, P. J. (1991) Prevention of Nitrofurantoin-Induced Cytotoxicity in Isolated Hepatocytes by Fructose. *Arch. Biochem. Biophys. 289*, 313-318.

[34] Lin, D., Guo, X., Gao, H., Cheng, L., Cheng, M., Song, S., Peng, Y., Zheng, J. (2015) *In vitro* and *in vivo* studies of the metabolic activation of 8-epidiosbulbin E acetate, *Chem. Res. Toxicol. 28*, 1737–1746.

[35] Li, W., Lin, D., Gao, H., Xu, Y., Meng, D., Smith, C. V., Peng, Y., Zheng, J. (2016) Metabolic activation of furan moiety makes diosbulbin B hepatotoxic. *Arch. Toxicol. 90*, 863-872.

[36] Boelsterli, U.A., Zhou, H.S., and Leow, K.Y. (2006) Bioactivation and Hepatotoxicity of Nitroaromatic Drugs. *Curr. Drug Metab. 7*, 715-727.

[37] Klee, S., Nürnberger, M.C., and Ungemach, F.R. (1994) The consequences of nitrofurantoin-induced oxidative stress in isolated rat hepatocytes: evaluation of pathobiochemical alterations. *Chem-Biol. Interact. 93*, 91-102.

[38] Rao, D.N., Jordan, S., Mason, R.P. (1988) Generation of nitro radical anions of some 5-nitrofurans, and 2- and 5-nitroimidazoles by rat hepatocytes. *Biochem. Pharmacol. 37*, 2907-2913.

[39] Rossi, L., Silva, J.M., McGirr, L.G., O'Brien, P.J. (1988) Nitrofurantoin-mediated oxidative stress cytotoxicity in isolated rat hepatocytes. *Biochem. Pharmacol. 37*, 3109-3117.

Table 1. Mass spectrometric profiling data obtained from LC-FT-ICR MS analysis of rat liver incubation mixtures in the presence of NFT, NADPH and GSH.

		$[M+H]^+$	$[M+H]^+$		
Compound	**Ion Formula**	**Calculated**	**Detected**	**Err[ppm]**	**Score**
M1	$C_{18}H_{24}N_7O_{10}S$	530.12999	530.13174	-3.3	100.00
M2	$C_{18}H_{24}N_7O_9S$	514.13507	514.13619	-2.2	100.00

Figure legends

Figure 1. Chemical structures of NFT, **1-9** and **4a**

Figure 2. GSH remaining and GSSG formation in rat liver microsomal incubations with NFT and test compounds **1-9**

Figure 3. GSH depletion mediated by NFT and test compounds **1-9, 4a** (A for NFT, **1-9**, **4a**; B for **4** and **4a**) in rat liver microsomal incubations. *$p < 0.05$, **$p < 0.01$ were considered significantly different. Labels * and ** on the bars represent significance between treated sample vs control. The horizontal lines with * or ** above the lines represent significance between different treatments. Data are mean ± SD; n=5

Figure 4. Cytotoxicity of NFT and test compounds **1-9, 4a** (A for NFT, **1-9**, **4a**; B for **4** and **4a**) in primary rat hepatocytes. *$p < 0.05$, **$p < 0.01$ were considered significantly different. Labels * and ** on the bars represent significance between treated sample vs control. The horizontal lines with * or ** above the lines represent significance between different treatments. Data are mean ± SD; n=3

Figure 5. Molecular electrostatic potential (MEP) surfaces property of NFT and **1-5** on same MEP scale. The color ramp for EP ranges from red (most positive; 51.4 kcal/mol) to purple (most negative; -56.0 kcal/mol)

Figure 6. Partial charges on the nitrogen atom of the nitro-containing compounds: NFT and test compounds **1-5**

Figure 7. Extracted ion (*m/z* 530→308) chromatograms obtained from LC-MS/MS

analysis of rat liver microsomal incubations containing NFT and GSH in the absence (A) or presence (B) of NADPH. (C) MS/MS spectrum of M1 generated in microsomal incubations. Extracted ion (*m/z* 514→162) chromatograms obtained from LC-MS/MS analysis of rat liver microsomal incubations containing NFT and GSH in the absence (D) or presence (E) of NADPH. (F) MS/MS spectrum of M2 generated in microsomal incubations

Figure 8. High-resolution mass spectra of M1 and M2

Fig. 1.

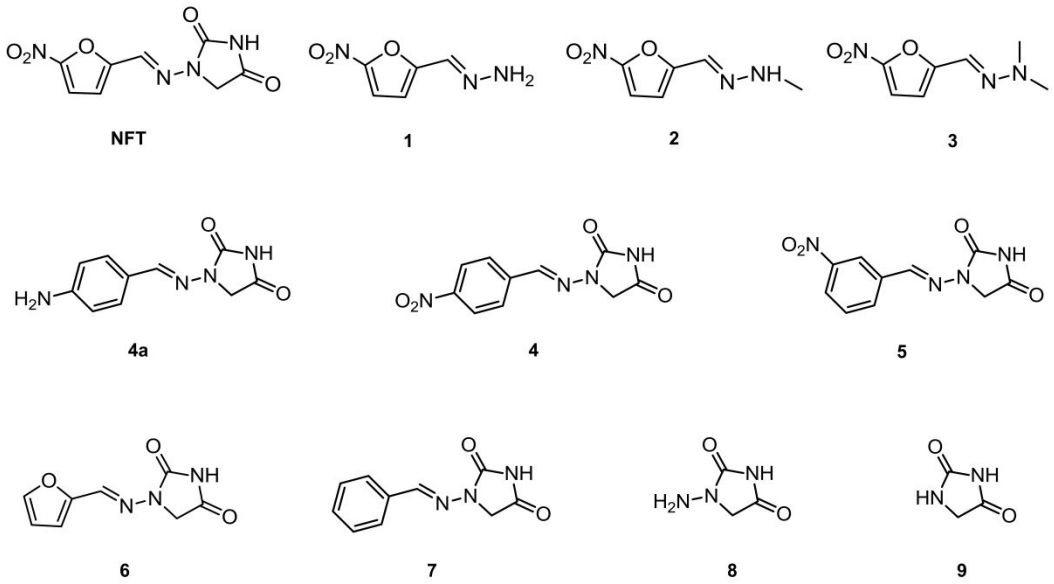

Fig.2.

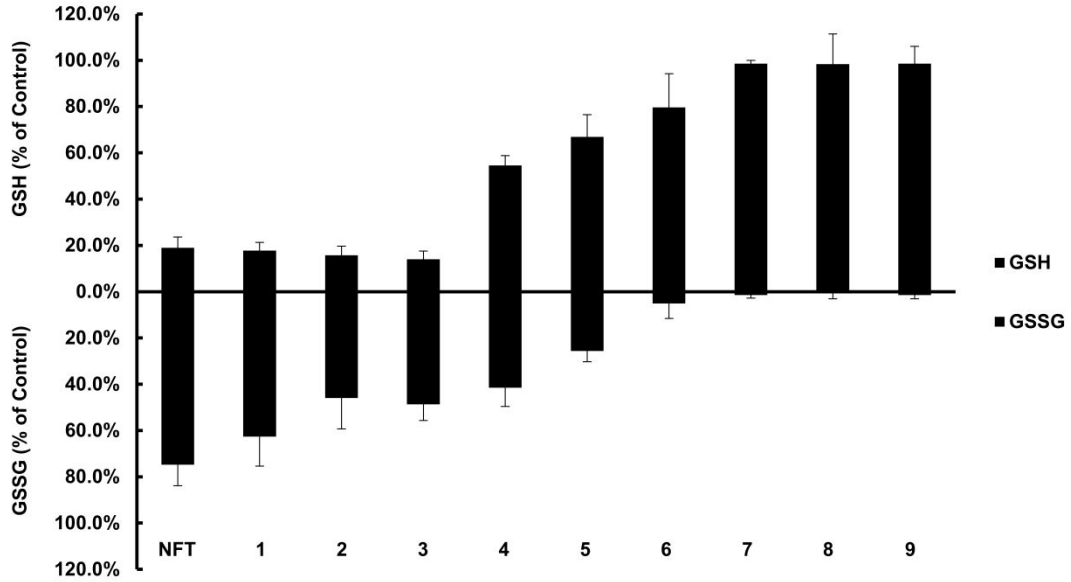
GSH (% of Control)
GSSG (% of Control)
120.0%
100.0%
80.0%
60.0%
40.0%
20.0%
0.0%
20.0%
40.0%
60.0%
80.0%
100.0%
120.0%
NFT
1
2
3
4
5
6
7
8
9
GSH
GSSG

Fig.3.

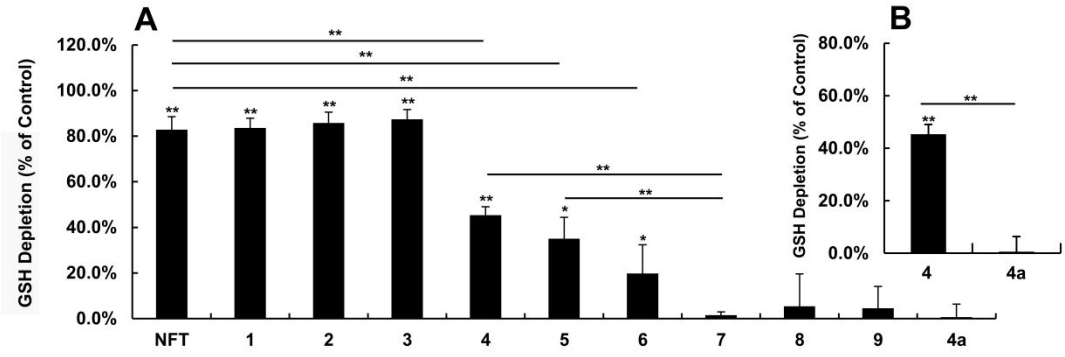
A
B
GSH Depletion (% of Control)
120.0%
100.0%
80.0%
60.0%
40.0%
20.0%
0.0%
NFT
1
2
3
4
5
6
7
8
9
4a
**
*

Fig.4.

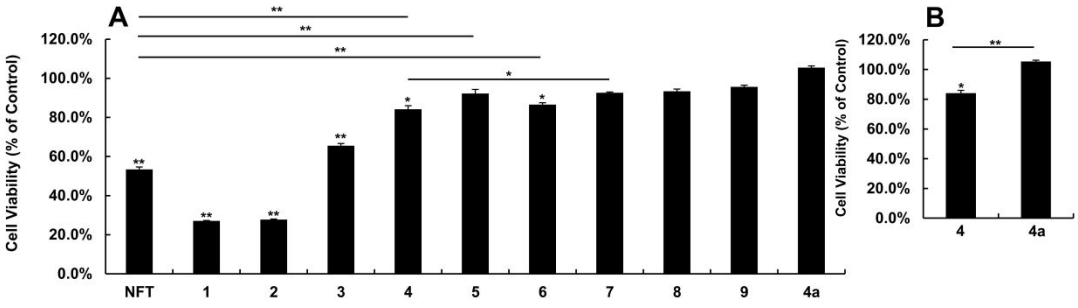
A
B
Cell Viability (% of Control)
120.0%
100.0%
80.0%
60.0%
40.0%
20.0%
0.0%
NFT
1
2
3
4
5
6
7
8
9
4a
4
4a

Fig.5.

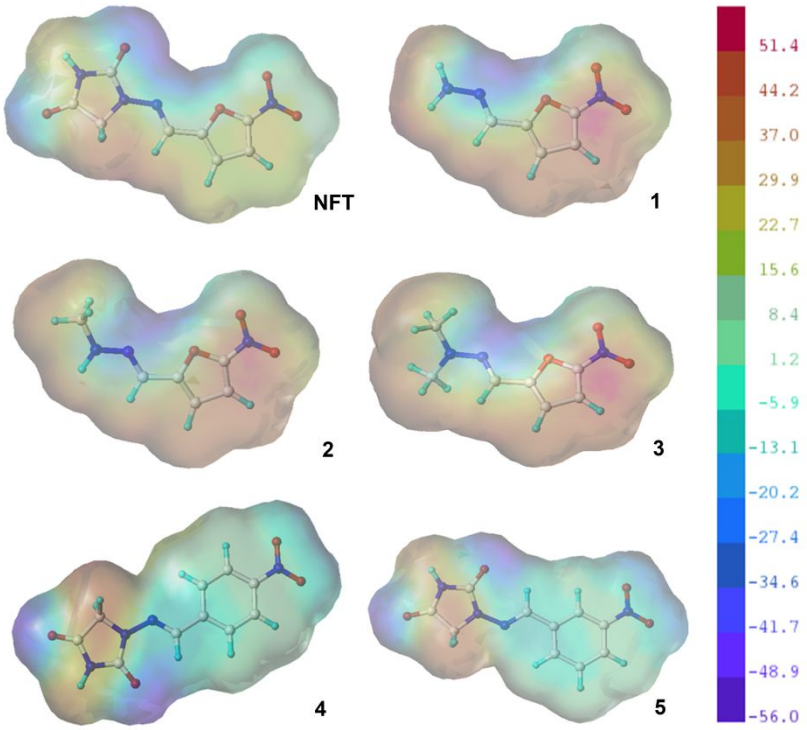
NFT
1
2
3
4
5
51.4
44.2
37.0
29.9
22.7
15.6
8.4
1.2
-5.9
-13.1
-20.2
-27.4
-34.6
-41.7
-48.9
-56.0

Fig.6.

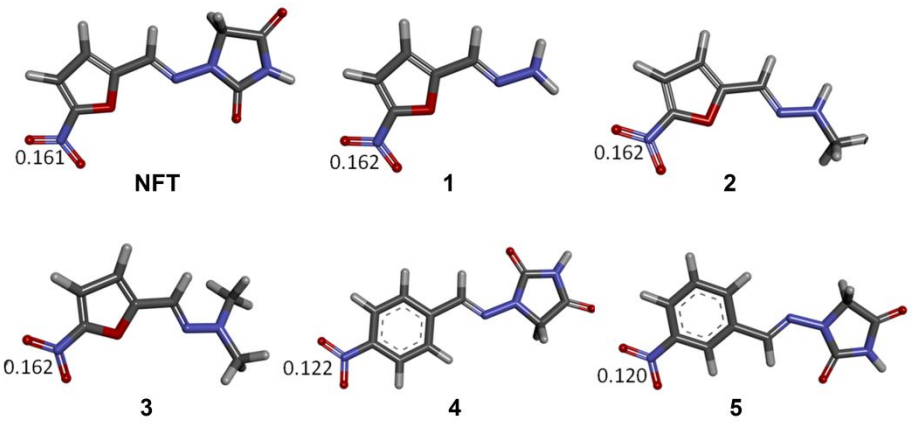

Fig.7.

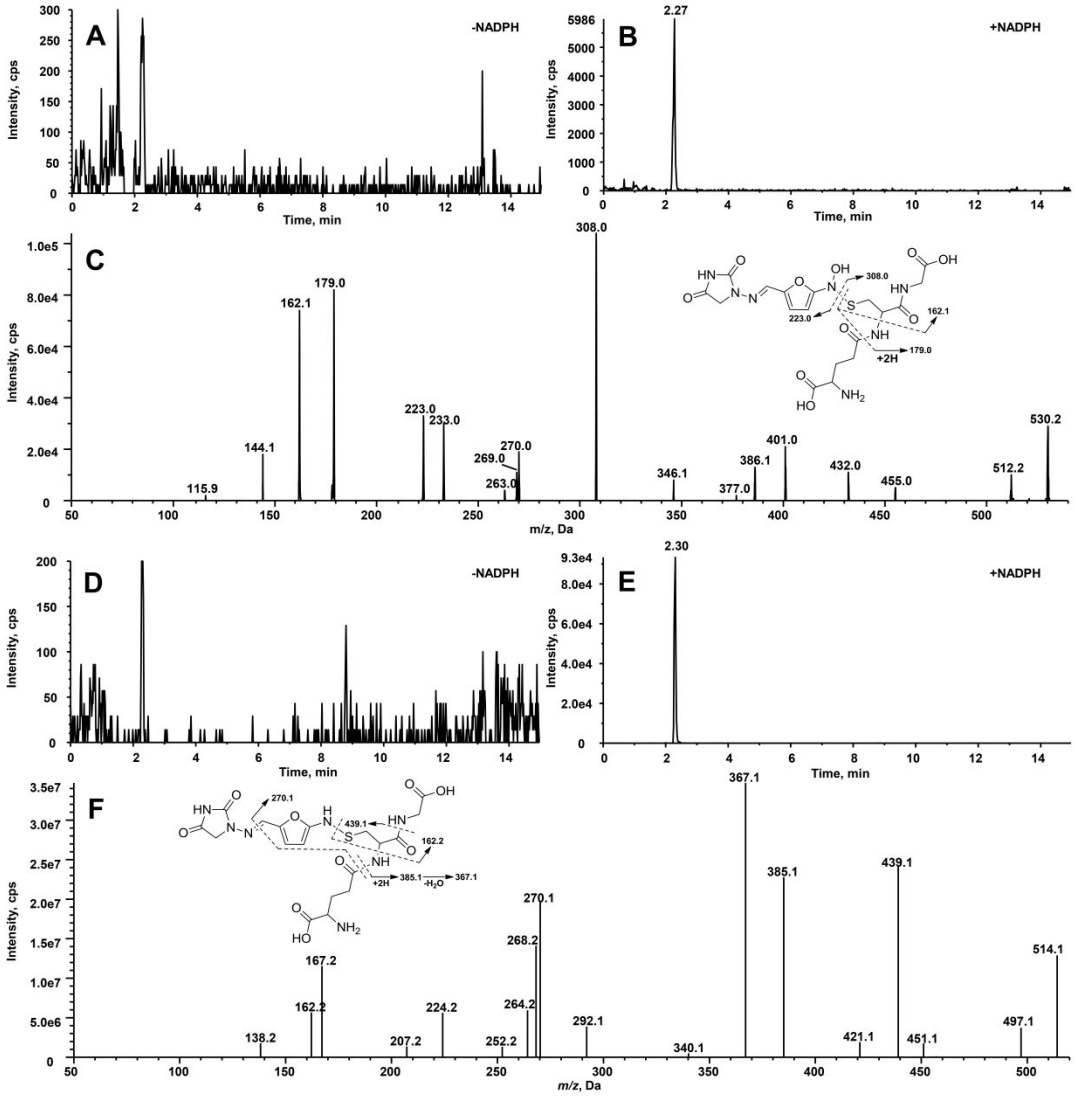
A
-NADPH
Intensity, cps
Time, min
B
+NADPH
2.27
C
308.0
179.0
162.1
223.0
233.0
144.1
270.0
269.0
263.0
115.9
346.1
386.1
401.0
432.0
455.0
377.0
512.2
530.2
m/z, Da
+2H
D
-NADPH
E
+NADPH
2.30
F
367.1
385.1
439.1
270.1
268.2
167.2
162.2
224.2
264.2
292.1
514.1
497.1
421.1
451.1
340.1
138.2
207.2
252.2
m/z, Da

Fig.8.

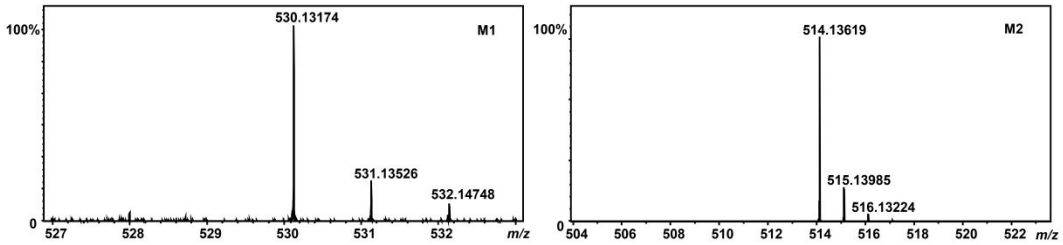
100%
530.13174
M1
531.13526
532.14748
0
527
528
529
530
531
532
m/z
100%
514.13619
M2
515.13985
516.13224
0
504
506
508
510
512
514
516
518
520
522
m/z

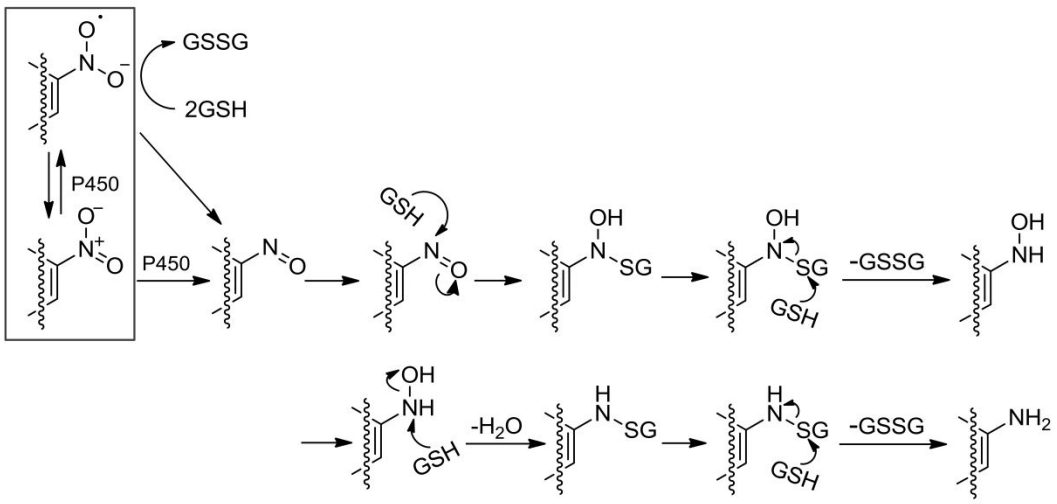

Scheme 1. Proposed mechanisms of P450- and GSH-mediated reduction of nitroaromatics